

Harnessing adapted capsule networks for accurate lumpy skin disease diagnosis in cattle

Goddeti Mallikarjun¹, V. A. Narayana²

¹Department of Computer Science and Engineering, Jawaharlal Nehru Technological University Hyderabad, Hyderabad, India

²Department of Computer Science and Engineering, CMR College of Engineering and Technology, Hyderabad, India

Article Info

Article history:

Received Feb 1, 2024

Revised Jun 22, 2024

Accepted Jun 28, 2024

Keywords:

Adapted capsule network
Histogram of oriented gradients
Invariant feature transform
Local binary patterns
Lumpy skin disease scale

ABSTRACT

Lumpy skin disease (LSD) poses a substantial risk to livestock, emphasizing the critical need for reliable diagnostic tools to ensure timely intervention. The considerable economic impact of LSD further accentuates the imperative for efficient diagnosis. In this context, artificial intelligence (AI) emerges as a transformative solution, playing a pivotal role in providing swift detection capabilities. Rapid identification of LSD not only alleviates economic burdens but also impedes the disease's propagation within herds. A ground breaking in iterative involves the implementation of an adapted capsule network (CapsNet) expressly designed for diagnosing LSD. This innovative strategy is finely tuned to discern intricate patterns in disease manifestation, achieving an impressive accuracy rate of 97.6%. The model's effectiveness is evident in its capacity to differentiate between infected and healthy cases, with precision, recall, and F1 score metrics registering at 9.65%, 97.1%, and 96.3%, respectively. This high level of precision underscores the model's proficiency in minimizing errors, solidifying its role as a dependable tool for precise LSD diagnosis and intervention, contributing significantly to the overall health and economic well-being of livestock populations.

This is an open access article under the [CC BY-SA](#) license.



Corresponding Author:

Goddeti Mallikarjun

Department of Computer Science and Engineering, Jawaharlal Nehru Technological University Hyderabad
Kukatpally, Hyderabad, Telangana, India

Email: goddeti.mallikarjun@gmail.com

1. INTRODUCTION

Lumpy skin disease (LSD) is a transmittable viral disease that mostly impacts cattle. The cause is the lumpy skin disease virus (LSDV), a member of the capripoxvirus genus in the poxviridae family. LSD has a long record of spreading across continents, first in Zambia in 1929 and expanding to Botswana 1943 [1]. In 1957, it had significant consequences in South Africa, affecting almost eight million cattle. The disease spread continuously, reaching Kenya in the same year, Sudan by 1970, and Nigeria by 1974 [2]. Outbreaks occurred in Mauritania, Mali, Ghana, and Liberia in 1977. Between 1981 and 1986, there were LSD outbreaks in Tanzania, Kenya, Zimbabwe, Somalia, and Cameroon, with a fatality rate of approximately 20%. LSD expanded to Egypt and Israel from Africa in 1988-1989 [3]. In 2012, its presence in southeastern Europe impacted both EU member states and the Balkans. Recent events in Asia, particularly in China, India, and Southeast Asian countries, underscore the alarming global spread of LSD [4].

LSD was discovered in India in November 2019, initially appearing sporadically in regions such as Odisha. Discrepancies from the 2019 outbreak were observed. Kerala documented instances from December 2019 to January 2021, while Assam recorded cases in August 2020 [5]. In April 2022, Gujarat reported cases that led to the implementation of cattle movement prohibitions in specific districts. After limitations were imposed in Rajasthan, Panchkula, Uttar Pradesh, and Madhya Pradesh, Maharashtra reported it as first

incidence in August 2022 [6]. Mumbai implemented a ban on cattle travel on September 14, followed by Uttar Pradesh implementing additional restrictions on September 2023. Chhattisgarh and Delhi implemented preventive measures and vaccination programs [7]. As of 2022, in India, LSD has significantly impacted the livestock population, with around 2.4 million animals infected and approximately 110,000 deaths reported. This highlights the seriousness of the disease's influence on the Indian agricultural sector, stressing the immediate requirement for efficient control and preventive actions to reduce its spread and lessen economic damages [8], [9]. The livestock industry is a crucial component of India's economy, supporting the livelihoods of millions and making a substantial contribution to agricultural production. LSD poses significant economic repercussions. This viral illness, mostly spread by blood-feeding insects like flies, mosquitoes, and ticks, poses a significant problem for India's cattle. Symptoms consist of fever and the formation of skin nodules, frequently resulting in death, particularly in cattle with no previous contact with the virus [5], [10].

Timely identification of LSD is essential for reducing its economic consequences and protecting the livestock sector. AI-driven diagnostic technologies show potential for speeding up detection procedures and delivering dependable, repeatable outcomes [11]. AI's effectiveness in identifying a range of human conditions, such as heart disease and skin cancer, and its use in diagnosing lumpy skin disorders show great potential [12]. Capsule networks (CapsNets) are highly relevant in diagnosing LSD by using photographs of the condition as a primary dataset. CapsNets excel at identifying spatial hierarchies and delicate details in medical photos of affected animals by utilizing advanced feature extraction techniques [13], [14]. Their exceptional capacity to generalize and interpret information makes them great tools for precisely identifying LSD-associated skin lesions. This emphasizes the essential requirement for CapsNets in diagnosing lumpy skin conditions.

2. LITERATURE REVIEW

Genemo [15] employed convolutional neural network (CNN) models, specifically DenseNet201 and region-based convolutional neural network (RCNN), for robust LSD diagnosis. Utilizing diverse classifiers like naive Bayes (NB), support vector machine (SVM), fine k-nearest neighbors (KNN), and extreme learning machines (ELM), the study achieved a notable 90.12% accuracy, with ELM proving most effective. Despite potential computational intensity and limited interpretability, Genemo's approach, leveraging varied feature extraction techniques, provides a comprehensive understanding of the disease from image data.

Lake *et al.* [16] employed a CNN-based approach for LSD diagnosis, achieving a commendable 95% accuracy after 50 epochs. The method showcased deep learning's efficacy in autonomously extracting intricate features for precise disease identification, emphasizing the model's ability to capture spatial hierarchies. Rony *et al.* [17] utilized CNN architectures, Inception V3, and VGG-16, achieving a notable 95% accuracy in LSD diagnosis. The use of these established architectures highlights CNNs' strength in automatic feature learning, contributing to effective image analysis. Inception V3's intricate pattern capture and VGG-16's fine-grained feature extraction enhance diagnostic potential. Rai *et al.* [18] investigation into LSD diagnosis incorporated CNN feature extraction techniques, utilizing VGG16, VGG19, and Inception V3, alongside diverse classifiers like KNN, SVM, NB, artificial neural network (ANN). The study achieved a notable 92.5% accuracy, with the most effective combination being ANN and Inception V3. Positive aspects include the versatility of feature extraction methods demonstrated by multiple CNN architectures.

Challenges across these studies include potential computational intensity, especially with advanced neural networks like DenseNet201 and RCNN and Inception V, raising concerns about resource requirements. Additionally, limited model interpretability is a common challenge, particularly in CNN-based approaches, where the "black-box" nature hinders understanding. The reliance on high-quality training data poses another challenge, requiring access to diverse and representative datasets. Balancing computational efficiency, model transparency, and potential overfitting, especially with complex models like Inception V3, remains a crucial consideration.

2.1. Problem statement

Cattle diseases threaten agriculture, causing economic losses and compromising animal welfare. Traditional manual detection methods are time-consuming and prone to errors. To address this, we propose a machine learning model that will analyze real-time visual symptoms, recognize patterns to diagnose individual animals, enable timely intervention, and enhance disease management and prevention in herds.

3. METHOD

In the preprocessing phase, raw image data undergoes various transformations to enhance the features relevant to nodular lesions. Techniques such as contrast enhancement, noise reduction, and image

normalization are applied to improve image quality and highlight distinctive characteristics. Additionally, feature extraction methods are employed to extract relevant information from the preprocessed images, focusing on nodular patterns and textures indicative of LSD.

The training process involves feeding the preprocessed images into the CapsNets architecture, along with corresponding disease labels. During training, the network learns to recognize nodular lesions as key indicators of the disease through iterative optimization of its parameters. After training, the model is evaluated using a separate dataset reserved for testing. The testing process involves presenting unseen images to the trained network and assessing its performance in correctly identifying nodular lesions indicative of LSD. Performance metrics such as accuracy, sensitivity, and specificity are calculated to evaluate the model's diagnostic capabilities as shown in Figure 1. Additionally, the model's interpretability allows clinicians to understand the reasoning behind its predictions, enhancing trust and its ability in clinical settings. Through rigorous training and testing, the CapsNets demonstrates its potential as an effective tool for early and accurate diagnosis of LSD based on nodular skin lesions.

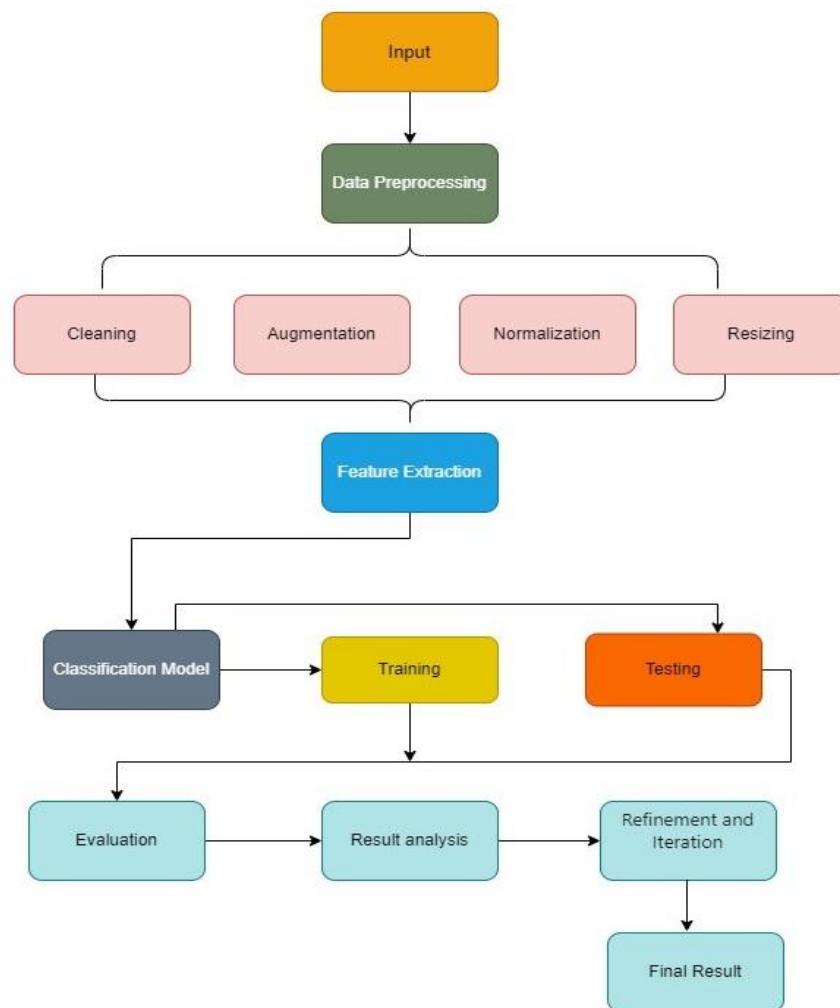


Figure 1. Proposed methodology for diagnose LSD

3.1. Data collection

A rigorous compilation of a comprehensive dataset of 520 RGB photographs was undertaken, sourced from various institutions such as P. V. Narasimha Rao Telangana Veterinary University, veterinary hospitals, and discussions with practitioners. In the present compilation, a total of 355 photographs depicts animals in a state of typical well-being, whereas 165 images showcase instances of lumpy skin illness. This comprehensive collection serves as a useful asset for veterinary research efforts, providing a strong basis for the advancement and enhancement of diagnostic instruments and therapeutic approaches.

3.2. Data pre-processing

The preparatory phase of data pre-processing played a pivotal role in enhancing the diagnostic capabilities of the collected images for LSD. The process included meticulous steps such as image cleaning, eliminating artifacts and irrelevant details to refine the dataset's quality. Normalization followed, standardizing pixel values across images, ensuring uniformity, and minimizing variations that could impact model training. Augmentation techniques were employed to introduce diversity, exposing the CapsNet to a broader spectrum of image variations and improving its generalization capabilities. Resizing the images to a standardized 256×256 resolution not only optimized computational efficiency but also provided a consistent input size for the CapsNet, streamlining the learning process.

3.3. Data annotation

Data annotation involves labeling a dataset for machine learning, often with class labels. 520 images categorized into two classes (normal: 0, diseased: 1, comprising 355 normal and 165 LSD images), this annotation provides critical information for disease diagnosis. The labeled dataset serves as a training ground for machine learning models, like CapsNets. By learning patterns associated with normal and diseased conditions, the model becomes proficient in distinguishing between the two, aiding in automated diagnosis.

3.5. Adapted CapsNet

The CapsNet has been rebranded as the adapted CapsNet, reflecting strategic modifications for enhanced performance in diagnosing LSD. These modifications include the integration of advanced feature extraction techniques and the incorporation of intermediate layers. These strategic enhancements empower the network to capture and interpret intricate patterns associated with the disease, resulting in improved diagnostic accuracy illustrated in Figure 2.

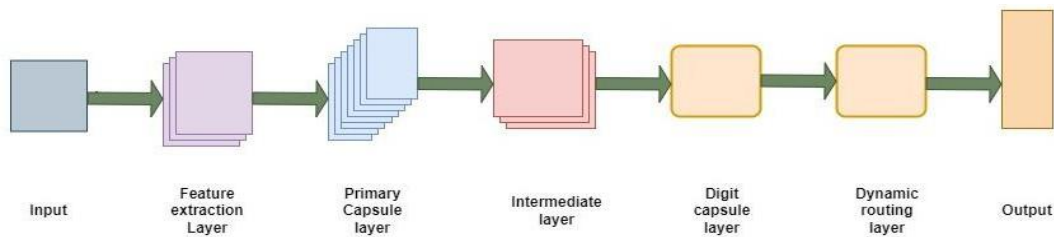


Figure 2. Adapted CapsNet architecture

3.6. Feature extraction layer

The specialized application of the scale-invariant feature transform (SIFT) is tailored for diagnosing LSD in cattle through advanced image analysis. It begins by detecting stable key points in images of cattle affected by LSD. SIFT then assigns orientations to these key points based on local gradient information, ensuring rotational invariance [19], [20].

Local binary pattern (LBP), a specialized texture descriptor, plays a crucial role in diagnosing LSD in cattle through nuanced image analysis. LBP's primary purpose is to encode local patterns in images by systematically comparing the intensity of a central pixel with that of its neighboring pixels [21]. The comparison yields binary codes, assigning '1' if the neighbor's intensity is greater or equal and '0' otherwise. These binary codes are then concatenated to form comprehensive binary patterns, encapsulating crucial texture information around each pixel [22].

Histogram of oriented gradients (HOG) is a pivotal component in the diagnostic arsenal for LSD in cattle, effectively capturing and representing gradient information related to shape and edge characteristics in images [23]. The process involves calculating the gradient magnitude and orientation for each pixel, followed by segmenting the image into small cells where gradient information is accumulated. Histograms of gradient orientations are then generated for each cell, emphasizing prevalent gradient directions that signify underlying patterns [24].

3.7. Primary capsule layer

Primary capsule layers play a crucial role in diagnosing LSD within a CapsNet architecture comprising 16 layers. These layers act as feature extractors, detecting low-level patterns and forming capsules responsible for encoding specific aspects of skin lesions. In the context of LSD, primary capsule layers likely

capture fundamental features such as textures, edges, and basic shapes associated with nodular skin lesions [25]. By utilizing 16 layers, the network can hierarchically learn increasingly complex features, enabling a nuanced understanding of the visual cues' indicative of the disease [26]. Squashing function:

$$\text{Squash}(x) = \frac{\|x\|^2}{1 + \|x\|^2} \quad (1)$$

The squash function normalizes the length of the vector as in (1), ensuring that the output is a unit vector.

3.8. Intermediate layer

The intermediate capsule layers serve as essential components for encoding abstract features in a hierarchical manner. Intermediate capsules act as intermediaries in the learning process, ensuring that the network captures increasingly intricate features related to the disease. Within this framework, the texture capsule layer assumes the task of honing in on fine-grained textural details embedded in the images [27]. This layer is designed to recognize and highlight specific textures that maybe indicative of pathological conditions. By focusing on capturing patterns related to texture, the texture capsule layer enhances the network's sensitivity to subtle variations and irregularities specific to the disease's textural characteristics. Complementing the texture capsule layer, the shape capsule layer specializes in extracting information pertinent to the overall shape, contour, and structural aspects of objects within the images [28], [29].

3.9. Digit capsule layer

Each digit capsule within the layers dedicated to capturing unique visual cues, employing dynamic routing mechanisms to hierarchically encode spatial hierarchies and nuanced features specific to different disease classes. The output vectors from the digit capsule layer provide a class-specific representation, contributing to a more focused and interpretable diagnosis. This approach improves the overall interpretability and accuracy of the CapsNet in identifying and categorizing different classes of LSD in cattle [30].

3.10. Dynamic routing layer

In the context of diagnosing LSD using a CapsNet, the dynamic routing layer, serving as the output layer, employs the SoftMax activation to calculate coupling coefficients (C_{ij}) based on agreement scores (S_{ij}) as in (2). This dynamic routing process is crucial for refining capsule interactions and extracting hierarchical features associated with the disease. The iterative refinement of (C_{ij}) is determined by the SoftMax activation function applied to the initial agreement scores (S_{ij}):

$$C_{ij} = \text{Softmax}(b_{ij}) \quad (2)$$

Here, (b_{ij}) represents the initial logit values or logits, which are exponentiated and normalized using the SoftMax function to obtain the coupling coefficients. The final output vector (V_j) of a capsule is obtained by squashing the weighted sum of predictions from lower-level capsules based on the refined coupling coefficients. Subsequently, the probabilities ($P(y=j)$) for each disease class are computed using the SoftMax function applied to the lengths of the output vectors as in (3). This approach enhances the interpretability and accuracy of the CapsNet, allowing it to discern intricate spatial hierarchies and nuanced features associated with LSD for more robust and reliable diagnosis [31].

$$P(y = j) = \frac{e^{\|v_j\|}}{\sum_k e^{\|v_k\|}} \quad (3)$$

3.11. Spread loss

The purpose of the modified spread loss is to enhance the differentiation between positive classes, which indicate the existence of a disease, and negative classes, which indicate the absence of a sickness as in (4) illustrates the simplified version that emphasizes the establishment of a clear separation between the lengths of output vectors related to these classes. The loss function enhances classification effectiveness by highlighting the difference between illness presence and absence, leading to improved model performance in discriminating between the two classes. Mathematically expressed as (4):

$$\text{Lspread} = \text{MAX}(0, m + \|V_{\text{positive}}\| - \|V_{\text{negative}}\|)^2 \quad (4)$$

Where V_{positive} represents the output vector for the positive class (presence of LSD), V_{negative} represents the output vector for the negative class (absence of LSD), and m is a margin hyper parameter that determines the minimum desired separation between the lengths of the positive and negative class capsules.

4. EXPERIMENTAL RESULTS AND DISCUSSION

The application of SIFT for diagnosing LSD in cattle involves advanced image analysis tailored to identify disease-related key points. SIFT excels in detecting stable key points, invariant to scale changes and rotations, in images of affected cattle depicted in Figure 3(a). LBP, a specialized texture descriptor, plays a crucial role in nuanced image analysis for LSD diagnosis depicted in Figure 3(b). LBP systematically encodes local patterns by comparing the intensity of a central pixel with it is neighbors. Additionally, the HOG proves pivotal in capturing and representing gradient information related to shape and edge characteristics in cattle images affected by LSD depicted in Figure 3(c).

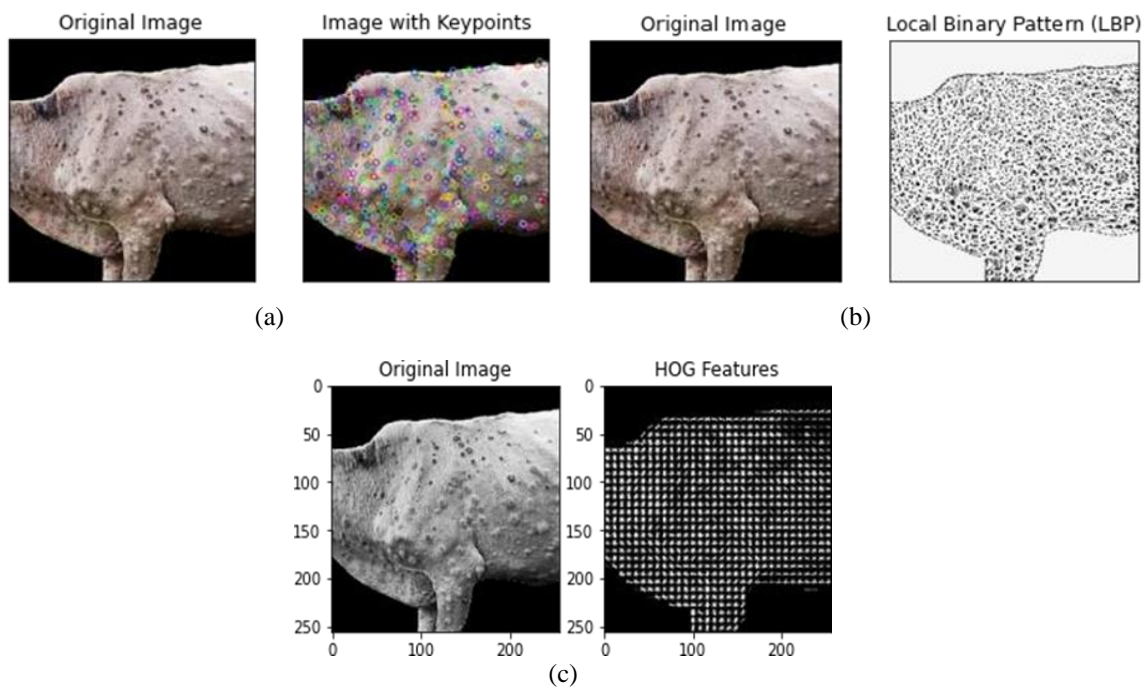


Figure 3. Sample results after applying feature extraction techniques: (a) SIFT, (b) LBP, and (c) HOG

4.1. Training results

Training outcomes for the CapsNet across ten epochs, each comprising 26 batches with 18 images per batch, demonstrate a compelling evolution in model performance. The progressive reduction in loss, starting at 0.20 in the first epoch and reaching a minimal 0.12 by the tenth epoch, reflects the model’s effective learning and consistent refinement of representations throughout training shown in Table 1. Concurrently, the ascending trajectory in training accuracy, rising from an initial 0.89 to an impressive 0.993 by the tenth epoch, underscores the network’s growing proficiency in precise classification within the training dataset. This upward trend highlights the model’s adaptability and its capacity to discern intricate patterns from the provided data illustrated in Figure 4.

Table 1. Training results			
Epoch	Batch	Loss	Training accuracy
1	8	0.20	0.89
2	5	0.16	0.92
3	7	0.39	0.93
4	1	0.30	0.91
5	9	0.20	0.94
6	15	0.31	0.96
7	22	0.36	0.97
8	21	0.11	0.98
9	2	0.51	0.98
10	23	0.10	0.99

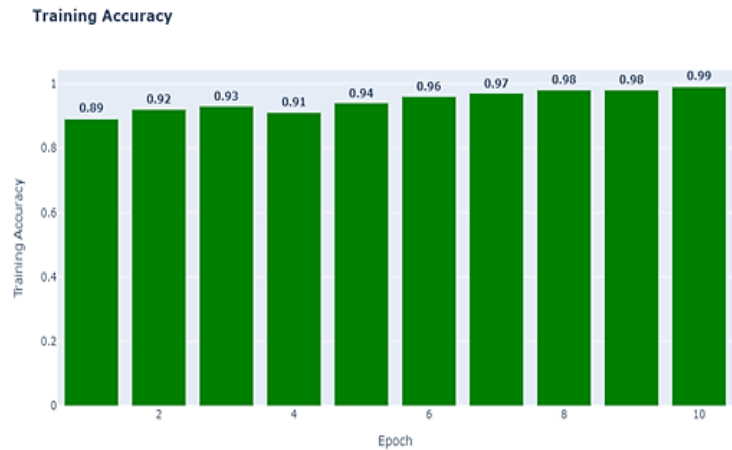


Figure 4. Training results accuracy

4.2. Hyperparameter

The primary goal of hyperparameter tuning was to precisely align the learning dynamics of the network with the complexities inherent in LSD data. Careful selection and configuration of hyperparameters, such as routing iterations, regularization techniques, and learning rate, aimed to strike a balance between underfitting and overfitting. This meticulous alignment ensures the network effectively learns and generalizes intricate patterns in the dataset. The outcome of these efforts, featuring a minimum learning rate of 0.1 and 16 primary capsules, highlights the success of hyperparameter tuning, resulting in an optimized CapsNet with enhanced diagnostic accuracy and robust generalization, as demonstrated in Table 2.

Table 2. Hyperparemeter tuning of adapted CapsNet

Hyperparameter	Values
Learning rate (lr)	0.1
Batch size	18
Number of primary capsules	16
Routing iterations	3
Regularization techniques	Capsule-wise drop out with rate 0.2
Loss function	Spread loss
Optimizer	Adam

The learning rate, set at 0.1, directs weight updates during training, ensuring a balanced convergence for optimal parameter values. A batch size of 18 facilitates efficient weight updates, aiding the network in generalizing LSD patterns. The choice of 16 primary capsules influences the network’s initial feature extraction for capturing essential visual cues. With 3 routing iterations, meaningful relationships between capsules refine hierarchical features associated with LSD. Capsule-wise dropout (rate 0.2) prevents overfitting, and the spread loss function guides diverse feature representation. The Adam optimizer ensures efficient weight updates, enhancing stability during the learning of complex disease patterns. In the pursuit of optimal learning dynamics, the learning rate was initially explored at minimal values, potentially reaching 0.01 or lower. However, it became evident that setting the learning rate to a minimum of 0.1 resulted in more efficient convergence and enhanced diagnostic accuracy. Simultaneously, the number of primary capsules underwent systematic variation, starting from a minimum, such as 4 or 8, and ultimately settling on 16.

4.3. Testing results

The testing results, a comprehensive evaluation of a CapsNets diagnostic prowess in LSD, are elucidated through key performance metrics across six batches. The quintessential metrics-accuracy, F1 score, precision, and recall-paint a vivid picture of the model’s effectiveness shown in Table 3. The CapsNets diagnostic prowess is quantified through various performance metrics, showcasing it is remarkable accuracy in identifying LSD. Accuracy, a foundational metric, steadily ascends across six batches, culminating in an impressive 97.6% accuracy in the final batch depicted in Figure 5(a). This upward trajectory underlines the model’s proficiency in correctly classifying instances of the disease, a testament to its ability to discern intricate patterns and features indicative of LSD.

Precision, a key aspect of the model's reliability, consistently demonstrates high values, reaching 96.3% depicted in Figure 5(b). This metric highlights the model's adeptness at minimizing false positives, ensuring that instances identified as LSD are indeed accurate. The precision score instills confidence in the diagnostic outcomes, emphasizing the model's capacity to differentiate genuine cases from false positives. The recall metric, measuring the model's ability to correctly identify all positive instances, exhibits an increasing trend, peaking at 96.8% depicted in Figure 5(c). This underscores the model's proficiency in capturing substantial proportion of actual LSD cases. The F1 score, a harmonious blend of precision and recall, provides a nuanced evaluation of the model's performance. The increasing trend in the F1 score, peaking at 96.6% depicted in Figure 5(d), signifies the model's ability to strike a balance between precision and recall.

Table 3. Testing results

Batch	Accuracy	F1score	Precision	Recall
1	0.935	0.945	0.939	0.948
2	0.941	0.947	0.943	0.952
3	0.948	0.954	0.951	0.958
4	0.950	0.956	0.952	0.962
5	0.961	0.966	0.962	0.968
6	0.976	0.963	0.965	0.971

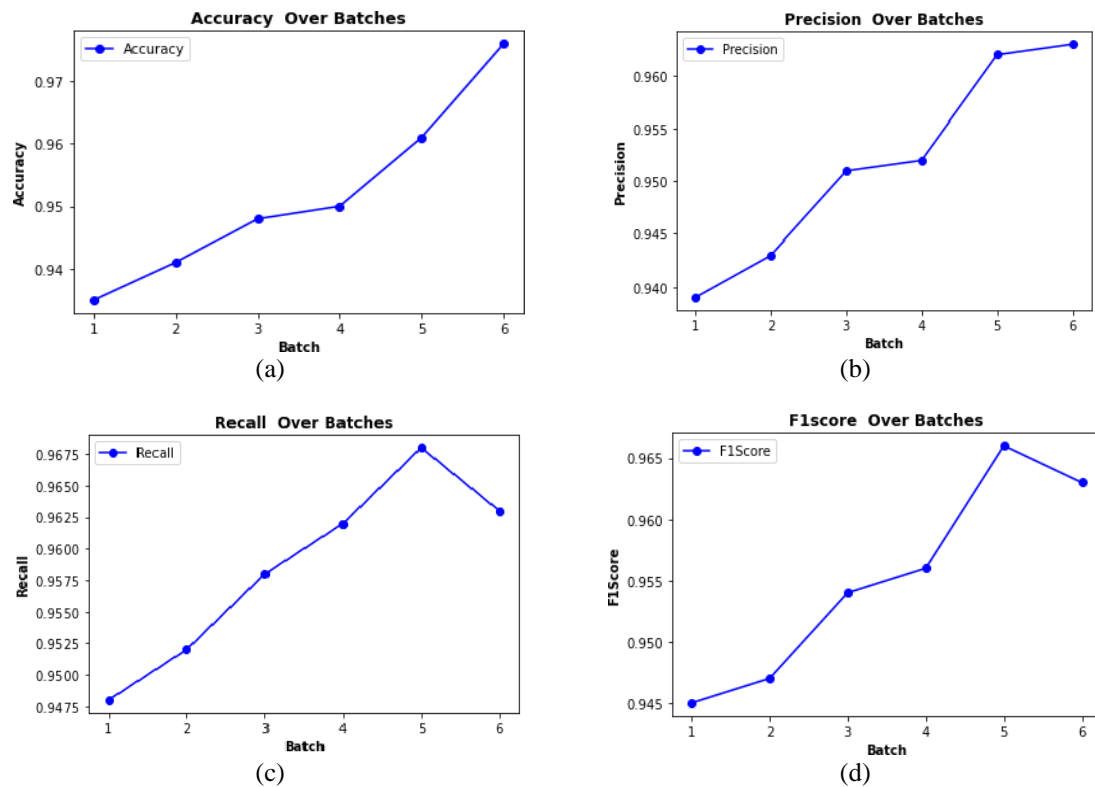


Figure 5. Testing results of CapsNet: (a) testing accuracy, (b) testing F1 score, (c) testing precision, and (d) testing recall

4.4. Confusion matrix

The performance of the model in diagnosing LSD is highly commendable, as evident from the confusion matrix. The model accurately identified 349 healthy instances (true negatives) and 159 diseased instances (true positives), showcasing its robust capability in correctly classifying both categories. The minimal counts of false positives (6) and false negatives (6) underscore the precision and recall of the model, highlighting its accuracy in minimizing misclassifications depicted in Figure 6. This balanced performance is indicative of the model's proficiency in distinguishing between affected and unaffected cases, a crucial aspect of an effective diagnostic tool depicted in Figure 6.

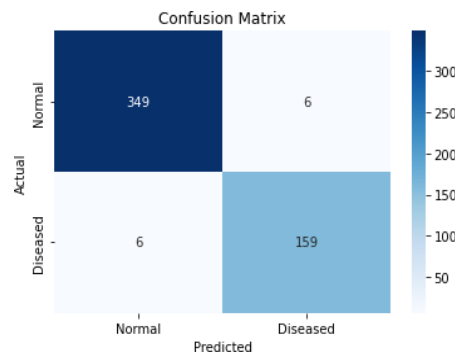


Figure 6. Confusion matrix of model performance

4.5. Receiver operating characteristic curve along with the area under the curve

The receiver operating characteristic (ROC) curve, along with an exceptional area under the curve (AUC) value of 0.9834, indicates a high level of diagnostic accuracy in detecting LSD. The model's high AUC highlights its ability to accurately differentiate between instances with diseases and those without, reducing the chances of misclassification, as seen in Figure 7. The model's sensitivity and specificity across different decision thresholds are further emphasized by the significant slope observed in the ROC curve. This observation implies that the model possesses the ability to accurately detect true positive cases while decreasing the occurrence of false positives, hence confirming its dependability in the diagnosis of LSD.

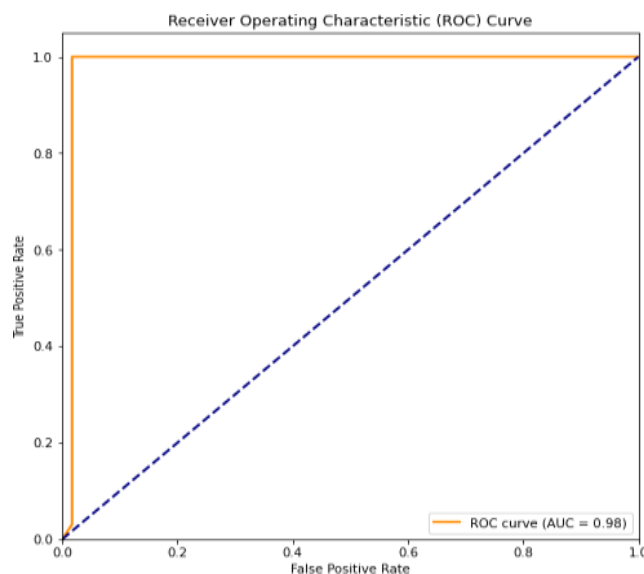


Figure 7. ROC curve along with the AUC

4.6. Matthew's correlation coefficient

The model's diagnostic accuracy in diagnosing LSD is shown by the Matthews correlation coefficient (MCC) obtaining a remarkable value of 0.9740. The model's high MCC demonstrates its exceptional capacity to accurately predict both genuine positives and true negatives, hence limiting the occurrence of false positives and false negatives. Utilizing a conservative threshold of 0.0100, the model exhibits an increased level of sensitivity towards even modest symptoms of disease, a critical factor in facilitating timely intervention and effective therapy. The robust performance of the system, especially when using a low threshold, indicates its reliability in detecting both overt and covert cases of LSD.

4.7. Comparing with existing work

The benchmark table provides a holistic view of various models' performances in a specific task, predominantly measured by accuracy. Among these models, the "adapted capsule network" stands out for its remarkable accuracy of 97.6%, indicating a finely tuned architecture tailored to meet the unique task

requirements. The “extreme learning machine” achieves a commendable accuracy of 90.12%, known for its simplicity and efficiency. A standalone “CNN” secures a solid 95% accuracy, leveraging its proficiency in capturing spatial hierarchies of features. The ensemble model, combining “CNN, InceptionV3, and VGG16 architectures,” also achieves 95% accuracy, showcasing the effectiveness of integrating multiple models. Lastly, the model fusing a “neural network with InceptionV3” attains a commendable accuracy of 92.5%, suggesting a synergy between the strengths of both architectures. In essence, this comparative analysis illustrates the versatility of different models and underscores the adapted CapsNets exceptional accuracy, positioning it as a promising candidate for precision-oriented tasks in real-world applications illustrated in Table 4. Validating the results of the adapted CapsNet involves comparing its diagnostic outcomes with assessments made by expert veterinary medical practitioners. By aligning the model’s predictions with the expert evaluations, we ensure a thorough and accurate examination of its performance in real-world scenarios.

Table 4. Comparing the proposed model with existing models

S. no	Author	Model	Accuracy (%)
1	Genemo [15]	ELM	90.12
2	Lake <i>et al.</i> [16]	CNN	95
3	Rony <i>et al.</i> [17]	CNN, Inception V3, and VGG-16	95
4	Rai <i>et al.</i> [18]	Neural network and inspectionv3	92.5
5	Proposed model	Adapted CapsNet	97.6

5. CONCLUSION

The adapted CapsNet has shown remarkable success in identifying LSD in cattle, with an outstanding accuracy rate of 97.6%. This exceeds current models, demonstrating its effectiveness and original design. Its distinctive capability to identify minor LSD-related patterns is a notable advancement in veterinary diagnostics. The model’s remarkable accuracy of 97.6% demonstrates its versatility and precision, establishing it as a leading tool in LSD diagnosis and possibly revolutionizing veterinary operations. Customized adjustments to the CapsNet structure have successfully addressed LSD diagnostic difficulties, making it a more dependable tool for veterinarians. The results provide promising opportunities for proactive control of LSD in bovine populations, facilitating prompt detection and response. This presents a hopeful structure for promptly identifying and reducing the impact of issues. In the future, there exists significant potential for more investigation into the scalability and use of the adapted CapsNet in other veterinary healthcare conditions. Exploring its wider range of uses could lead to substantial progress in AI-powered veterinary diagnostics. The study trajectory exhibits potential for transforming the field, potentially optimizing the processes of diagnosing and treating diverse animal health issues.

REFERENCES

[1] M. Akther *et al.*, “Global burden of lumpy skin disease, outbreaks, and future challenges,” *Viruses*, vol. 15, no. 9, Aug. 2023, doi: 10.3390/v15091861.

[2] G. Pandey *et al.*, “Molecular and serological detection of lumpy skin disease in cattle of Western Chitwan, Nepal,” *Proceedings of 12th National Workshop on Livestock and Fisheries Research in Nepal*, vol. 3, pp. 57-61, 2021.

[3] Z. Liang *et al.*, “Understanding the research advances on lumpy skin disease: A comprehensive literature review of experimental evidence,” *Frontiers in Microbiology*, vol. 13, Nov. 2022, doi: 10.3389/fmicb.2022.1065894.

[4] N. Kumar *et al.*, “Isolation and characterization of lumpy skin disease virus from cattle in India,” *Plos One*, vol. 16, no. 1, Jan. 2021, doi: 10.1371/journal.pone.0241022.

[5] E. Mathivanan, K. Raju, and R. Murugan, “Outbreak of lumpy skin disease in India 2022-an emerging threat to livestock and livelihoods,” *Global Biosecurity*, vol. 5, Feb. 2023, doi: 10.31646/gbio.187.

[6] S. B. Sudhakar *et al.*, “Lumpy skin disease (LSD) outbreaks in cattle in Odisha state, India in August 2019: Epidemiological features and molecular studies,” *Transboundary and Emerging Diseases*, vol. 67, no. 6, pp. 2408–2422, Nov. 2020, doi: 10.1111/tbed.13579.

[7] N. Kumar and B. N. Tripathi, “A serious skin virus epidemic sweeping through the Indian subcontinent is a threat to the livelihood of farmers,” *Virulence*, vol. 13, no. 1, pp. 1943–1944, Dec. 2022, doi: 10.1080/21505594.2022.2141971.

[8] G. B. M. Reddy *et al.*, “Lumpy skin disease (LSD) in Yak (*Bos grunniens*): an evidence of species spillover from Cattle in India,” *Microorganisms*, vol. 11, no. 12, 2023, doi: 10.3390/microorganisms11122823.

[9] S. E. Saqib, M. Yaseen, S. Visetnoi, Sikandar, and S. Ali, “Epidemiological and economic consequences of lumpy skin disease outbreaks on farm households in Khyber Pakhtunkhwa, Pakistan,” *Frontiers in Veterinary Science*, vol. 10, Dec. 2023, doi: 10.3389/fvets.2023.1238771.

[10] W. Molla, M. C. M. D. Jong, G. Gari, and K. Frankena, “Economic impact of lumpy skin disease and cost effectiveness of vaccination for the control of outbreaks in Ethiopia,” *Preventive Veterinary Medicine*, vol. 147, pp. 100–107, Nov. 2017, doi: 10.1016/j.prevetmed.2017.09.003.




[11] A. Rai, S. S. Rawat, H. Chopra, I. Singh, and T. B. Emran, “Lumpy skin disease: the underestimated epidemic for cattle in India,” *International Journal of Surgery: Global Health*, vol. 6, no. 5, Sep. 2023, doi: 10.1097/GH9.0000000000000282.

[12] Y. Kumar, A. Koul, R. Singla, and M. F. Ijaz, “Artificial intelligence in disease diagnosis: A systematic literature review, synthesizing framework and future research agenda,” *Journal of Ambient Intelligence and Humanized Computing*, vol. 14, no. 7, pp. 8459–8486, Jul. 2023, doi: 10.1007/s12652-021-03612-z.




- [13] V. R. Umapathy *et al.*, "Perspective of artificial intelligence in disease diagnosis: A review of current and future endeavours in the medical field," *Cureus*, vol. 15, no. 9, Sep. 2023, doi: 10.7759/cureus.45684.
- [14] G. Rangel, J. C. C. -Tello, M. Rivera, and O. Renteria, "A deep learning model based on capsule networks for COVID diagnostics through x-ray images," *Diagnostics*, vol. 13, no. 17, Sep. 2023, doi: 10.3390/diagnostics13172858.
- [15] M. Genemo, "Detecting high-risk area for lumpy skin disease in cattle using deep learning feature," *Advances in Artificial Intelligence Research*, vol. 3, no. 1, pp. 27–35, Feb. 2023, doi: 10.54569/air.1164731.
- [16] B. Lake, F. Getahun, and F. T. Teshome, "Application of artificial intelligence algorithm in image processing for cattle disease diagnosis," *Journal of Intelligent Learning Systems and Applications*, vol. 14, no. 4, pp. 71–88, 2022, doi: 10.4236/jilsa.2022.144006.
- [17] M. Rony, D. Barai, Riad, and Z. Hasan, "Cattle external disease classification using deep learning techniques," in *2021 12th International Conference on Computing Communication and Networking Technologies (ICCCNT)*, IEEE, Jul. 2021, pp. 1–7, doi: 10.1109/ICCCNT51525.2021.9579662.
- [18] G. Rai, Naveen, A. Hussain, A. Kumar, A. Ansari, and N. Khanduja, "A deep learning approach to detect lumpy skin disease in Cows," in *Computer Networks, Big Data and IoT*, 2021, pp. 369–377, doi: 10.1007/978-981-16-0965-7_30.
- [19] H. R. Kher and V. K. Thakar, "Scale invariant feature transform based image matching and registration," in *2014 Fifth International Conference on Signal and Image Processing*, IEEE, Jan. 2014, pp. 50–55, doi: 10.1109/ICSIP.2014.12.
- [20] T. Nguyen, E. -A. Park, J. Han, D. -C. Park, and S.-Y. Min, "Object detection using scale invariant feature transform," in *Genetic and Evolutionary Computing: Proceedings of the Seventh International Conference on Genetic and Evolutionary Computing, ICGEC 2013*, Prague, Czech Republic, 2014, pp. 65–72, doi: 10.1007/978-3-319-01796-9_7.
- [21] M. A. Muqet and R. S. Holambe, "Local binary patterns based on directional wavelet transform for expression and pose-invariant face recognition," *Applied Computing and Informatics*, vol. 15, no. 2, pp. 163–171, Jul. 2019, doi: 10.1016/j.aci.2017.11.002.
- [22] Y. Cai, G. Xu, A. Li, and X. Wang, "A novel improved local binary pattern and its application to the fault diagnosis of diesel engine," *Shock and Vibration*, vol. 2020, pp. 1–15, Feb. 2020, doi: 10.1155/2020/9830162.
- [23] N. Dalal and B. Triggs, "Histograms of oriented gradients for human detection," in *2005 IEEE Computer Society Conference on Computer Vision and Pattern Recognition (CVPR '05)*, IEEE, 2005, pp. 886–893, doi: 10.1109/CVPR.2005.177.
- [24] B. Bhattarai, R. Subedi, R. R. Gaire, E. Vazquez, and D. Stoyanov, "Histogram of oriented gradients meet deep learning: A novel multi-task deep network for 2D surgical image semantic segmentation," *Medical Image Analysis*, vol. 85, Apr. 2023, doi: 10.1016/j.media.2023.102747.
- [25] V. Mazzia, F. Salvetti, and M. Chiaberge, "Efficient-CapsNet: capsule network with self-attention routing," *Scientific Reports*, vol. 11, no. 1, Jul. 2021, doi: 10.1038/s41598-021-93977-0.
- [26] S. Panigrahi, J. Das, and T. Swarnkar, "Capsule network based analysis of histopathological images of oral squamous cell carcinoma," *Journal of King Saud University-Computer and Information Sciences*, vol. 34, no. 7, pp. 4546–4553, Jul. 2022, doi: 10.1016/j.jksuci.2020.11.003.
- [27] J. Peebles, W. Xu, and A. Zare, "Histogram layers for texture analysis," *IEEE Transactions on Artificial Intelligence*, vol. 3, no. 4, pp. 541–552, Aug. 2022, doi: 10.1109/TAI.2021.3135804.
- [28] C. Zhang, Y. Zheng, B. Guo, C. Li, and N. Liao, "SCN: A novel shape classification algorithm based on convolutional neural network," *Symmetry*, vol. 13, no. 3, Mar. 2021, doi: 10.3390/sym13030499.
- [29] Z. Liang, Z. Nie, A. An, J. Gong, and X. Wang, "A particle shape extraction and evaluation method using a deep convolutional neural network and digital image processing," *Powder Technology*, vol. 353, pp. 156–170, Jul. 2019, doi: 10.1016/j.powtec.2019.05.025.
- [30] M. U. Haq, M. A. J. Sethi, and A. U. Rehman, "Capsule network with its limitation, modification, and applications-a survey," *Machine Learning and Knowledge Extraction*, vol. 5, no. 3, pp. 891–921, Aug. 2023, doi: 10.3390/make5030047.
- [31] M. K. Patrick, A. F. Adekoya, A. A. Mighty, and B. Y. Edward, "Capsule networks-a survey," *Journal of King Saud University-Computer and Information Sciences*, vol. 34, no. 1, pp. 1295–1310, Jan. 2022, doi: 10.1016/j.jksuci.2019.09.014.

BIOGRAPHIES OF AUTHORS



Goddeti Mallikarjun    is research scholar in the Department of Computer Science and Engineering, Jawaharlal Nehru Technological University Hyderabad (JNTUH), Hyderabad, Telangana, India. His research interests are artificial intelligence, machine learning, and deep learning. He has published many articles in the field of machine learning application in the health care sector. He can be contacted at email: goddeti.mallikarjun@gmail.com.



V. A. Narayana    received a Ph.D. degree in computer science from Jawaharlal Nehru Technological University Hyderabad (JNTUH). He has been a Professor of Computer Science, in the Department of Computer Science and Engineering, CMRCET, Hyderabad, since 2006. His research interests are web mining, neural networks, and pattern recognition. He is currently the principal of CMR College of Engineering and Technology (CMRCET). He is a Fellow Institution of Engineers (India) and a member of various professional bodies. He can be contacted at email: vanarayana@cmrcet.org.